

Lawrence Berkeley National Laboratory

LBL Publications

Title

Electronic transport properties of spin-crossover polymer plus polyaniline composites with Fe₃O₄ nanoparticles

Permalink

<https://escholarship.org/uc/item/21x088n7>

Journal

Journal of Physics Materials, 7(1)

ISSN

2515-7639

Authors

Mishra, Esha
Chin, WaiKiat
McElveen, Kayleigh A
[et al.](#)

Publication Date

2024

DOI

10.1088/2515-7639/ad1b35

Copyright Information

This work is made available under the terms of a Creative Commons Attribution License, available at <https://creativecommons.org/licenses/by/4.0/>

Peer reviewed

PAPER • OPEN ACCESS

Electronic transport properties of spin-crossover polymer plus polyaniline composites with Fe₃O₄ nanoparticles

To cite this article: Esha Mishra *et al* 2024 *J. Phys. Mater.* **7** 015010

View the [article online](#) for updates and enhancements.

You may also like

- [Spin-crossover behavior of bis\(dihydrobis\(4-methylpyrazol-1-yl-borate\)\)-\(2,2-bipyridine\)iron and analogous complexes in the bulk and in thin films: Elucidating the influence of —interactions on the type of spin transition](#)
Sascha Ossinger, Christian Näther and Felix Tucek
- [Magneto-elastic properties of a spin crossover membrane deposited on a deformable substrate](#)
K Affes, A Slimani, Y Singh et al.
- [Investigation of iron spin crossover pressure in Fe-bearing MgO using hybrid functional](#)
Ya Cheng, Xianlong Wang, Jie Zhang et al.

PRIME
PACIFIC RIM MEETING
ON ELECTROCHEMICAL
AND SOLID STATE SCIENCE

HONOLULU, HI
Oct 6–11, 2024

Abstract submission
deadline extended:
April 19, 2024
Learn more and submit!

Joint Meeting of
The Electrochemical Society
•
The Electrochemical Society of Japan
•
Korea Electrochemical Society



PAPER

OPEN ACCESS

Electronic transport properties of spin-crossover polymer plus polyaniline composites with Fe₃O₄ nanoparticlesRECEIVED
14 July 2023REVISED
21 November 2023ACCEPTED FOR PUBLICATION
4 January 2024PUBLISHED
16 January 2024

Original Content from this work may be used under the terms of the [Creative Commons Attribution 4.0 licence](#).

Any further distribution of this work must maintain attribution to the author(s) and the title of the work, journal citation and DOI.



Esha Mishra^{1,2} , WaiKiat Chin¹ , Kayleigh A McElveen³ , Thilini K Ekanayaka¹ , M Zaid Zaz¹ , Gauthami Viswan¹ , Ruthi Zielinski¹ , Alpha T N'Diaye⁴ , David Shapiro⁴ , Rebecca Y Lai³ , Robert Streubel^{1,5,*} and Peter A Dowben^{1,*}

¹ Department of Physics and Astronomy, University of Nebraska-Lincoln, Lincoln, NE 68588, United States of America

² Department of Physics, Berry College, Mount Berry, GA 30149, United States of America

³ Department of Chemistry, University of Nebraska-Lincoln, Lincoln, NE 68588, United States of America

⁴ Advanced Light Source, Lawrence Berkeley National Laboratory, Berkeley, CA 94720, United States of America

⁵ Nebraska Center for Materials and Nanoscience, University of Nebraska-Lincoln, Lincoln, NE 68588, United States of America

* Authors to whom any correspondence should be addressed.

E-mail: streubel@unl.edu and pdowben@unl.edu

Keywords: molecular electronics, spin-crossover, electric conductivity, phase separation, magnetic nanoparticles

Supplementary material for this article is available [online](#)

Abstract

Adding Fe₃O₄ nanoparticles to composites of [Fe(Htrz)₂(trz)](BF₄) spin-crossover polymer and polyaniline (PANI) drives a phase separation of both and restores the molecular structure and cooperative effects of the spin-crossover polymer without compromising the increased conductivity gained through the addition of PANI. We observe an increased on-off ratio for the DC conductivity owing to an enlarged off state resistivity and a 20 times larger AC conductivity of the on state compared with DC values. The Fe₃O₄ nanoparticles, primarily confined to the [Fe(Htrz)₂(trz)](BF₄) phase, are ferromagnetically coupled to the local moment of the spin-crossover molecule suggesting the existence of an exchange interaction between both components.

1. Introduction

Composite materials are multi-component systems whose functionality is governed by the interplay between their constituents. The homogeneity of the compound depends on the materials, the materials interactions, and synthesis and profoundly affects properties. Nanoparticles have shown to promote mixing of immiscible liquids by becoming surfactants due to a reduction of interfacial tension [1] and may lead to a reversible transformation between immiscible and miscible polymer solutions. Adding magnetic nanoparticles to molecular ferroelectrics has enabled the synthesis of multiferroic materials [2–4]. There are few studies of adding magnetic nanoparticles to spin-crossover molecules, though spin-crossover complexes can form nanoparticles themselves [5–7]. One such spin-crossover complex is [Fe(Htrz)₂(trz)](BF₄) (Htrz = 1H-1,2,4-triazole, trz[−] = deprotonated triazolato ligand) [7–12] that also has been combined with nanoparticles [13, 14]. [Fe(Htrz)₂(trz)](BF₄) is characterized by a temperature-dependent spin-state switching causing a change in conductivity [9, 15–19]. The spin-crossover transition temperature of this particular molecule is typically (340–360) K yielding a bistability of spin states near room temperature [8–12, 15–20]. Through the addition of polyaniline (PANI) [19, 21] or polypyrrole [21, 22], the on-state resistance of the resulting homogeneous composite can be reduced to <1 Ω·cm so that smaller molecular devices become possible [23] without long delay times resulting from a high impedance. To understand modifications to cooperative effects governing the bistability between spin states [24] in spin-crossover complexes, a variety of techniques have been employed [25–27]. While metal substitutions for Fe in [Fe(Htrz)₂(trz)](BF₄) decreases conductivity [18], adding metallic nanoparticles like Fe₃O₄ may avoid this problem altogether through driving a morphology change. Leveraging the full potential of such multi-component systems and modifications due to the addition of nanoparticles requires a profound

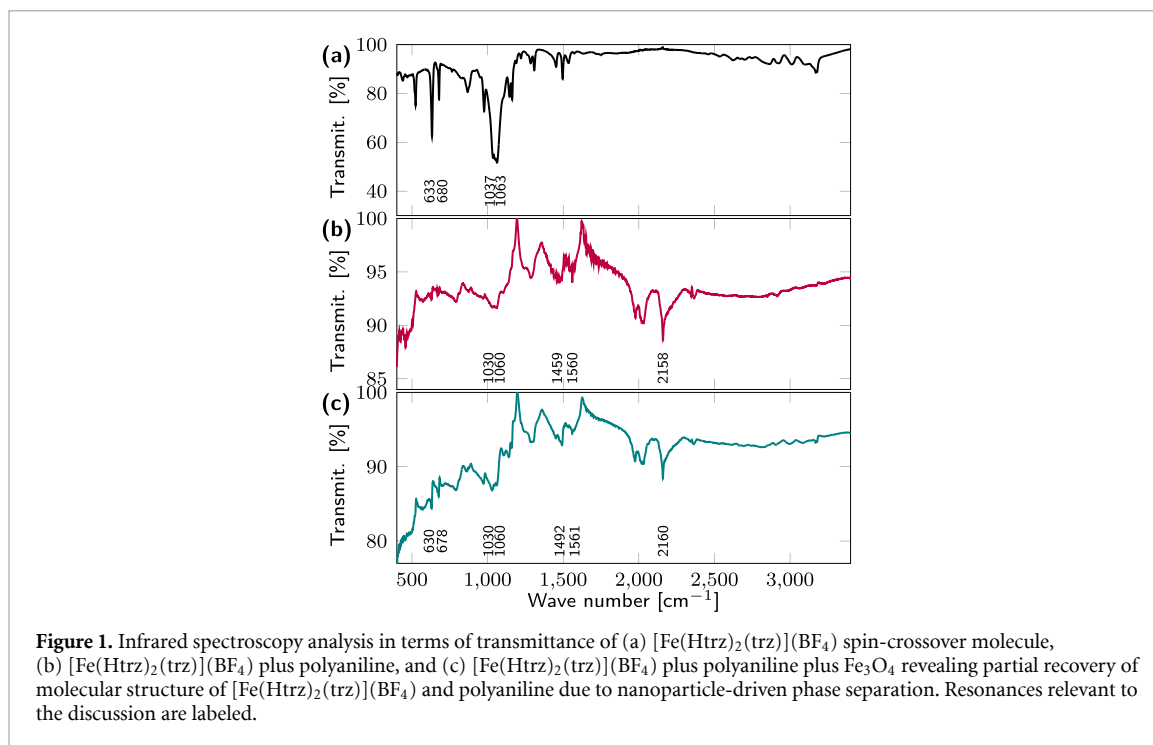
understanding of the paramagnetic correlation length and the coupling at the interface between superparamagnetic nanoparticles and polymers. Studies of this kind have been extremely rare [13, 14] and it is important to begin to address this deficiency in terms of magnetic and electronic transport characterization in conjunction with structural and chemical microanalysis.

Here, we report the effects of adding superparamagnetic nanoparticles to composite films of $[\text{Fe}(\text{Htrz})_2(\text{trz})](\text{BF}_4)$ spin-crossover molecules and PANI. Scanning transmission electron microscopy with energy-dispersive x-ray spectroscopy and scanning transmission x-ray spectromicroscopy confirm a phase separation of $[\text{Fe}(\text{Htrz})_2(\text{trz})](\text{BF}_4)$ and PANI that is driven by the Fe_3O_4 nanoparticles (1 weight-%), which primarily reside in the former phase. Infrared spectroscopy and magnetometry studies corroborate the restoration of molecular structure and cooperative effects after adding the nanoparticles without compromising the increased conductivity gained through the addition of PANI. In fact, DC and AC resistivity measurements divulge an increased on-off ratio for the DC conductivity by enlarging the resistivity of the high-spin state (off state) and a 20 times larger AC conductivity of the on state compared with DC values. Moreover, x-ray magnetic circular dichroism (XMCD) spectroscopy unveils ferromagnetic coupling between the local moment of $[\text{Fe}(\text{Htrz})_2(\text{trz})](\text{BF}_4)$ and Fe_3O_4 nanoparticles necessitating a complex exchange coupling between the disordered components.

2. Synthesis and molecular structure

The $[\text{Fe}(\text{Htrz})_2(\text{trz})](\text{BF}_4)$ spin-crossover polymer and PANI were synthesized following methods reported by Kroeber *et al* [20], Tang *et al* [28], and Adams and Hendrickson [29]. For $[\text{Fe}(\text{Htrz})_2(\text{trz})](\text{BF}_4)$, a 3 M solution of 1,2,4-triazole (Alfa Aesar) in anhydrous ethanol (Aldrich) was added to a stirring solution of $\text{Fe}(\text{BF}_4)_2 \cdot 6\text{H}_2\text{O}$ (Aldrich) in anhydrous ethanol at a rate of $30 \mu\text{l min}^{-1}$. The resulting pink suspension was stirred for an hour at room temperature and was kept overnight at ambient conditions. Then, the supernatant was removed and the pale pink solid was collected via gravity filtration and washed with anhydrous ethanol several times. For the PANI synthesis, a solution of 0.25 M aniline (Fisher Scientific) in 30 ml of water was placed in an ice bath and cooled to near 0°C while stirring. 10 ml of 0.25 M ammonium persulfate (Millipore Sigma) in 1 M HCl (Fisher Scientific) were added to the aniline solution in one step. The reaction mixture was stirred for six hours in the ice bath to promote polymerization. A dark green precipitate was noted after six hours, but the reaction mixture was left to stir overnight at room temperature. The next day, the dark green powder was collected via centrifugation at 4500 rpm for 30 min several times. The resulting PANI was rinsed with 1 M HCl, ethanol, and water. The $[\text{Fe}(\text{Htrz})_2(\text{trz})](\text{BF}_4)$ plus PANI composite was obtained after careful grinding with mortar and pestle to smooth powders separately. 25 mg of PANI (5000 g mol^{-1}) were dispersed in 2 ml of water and sonicated to a uniform dispersion upon which 25 mg of $[\text{Fe}(\text{Htrz})_2(\text{trz})](\text{BF}_4)$ ($348.67 \text{ g mol}^{-1}$) were added. The resulting suspension was sonicated and the water was allowed to evaporate overnight. Adding 1 weight-% Fe_3O_4 nanoparticles to the uniform mixture followed by 30 min sonication at room temperature yields the $[\text{Fe}(\text{Htrz})_2(\text{trz})](\text{BF}_4)$ plus PANI plus Fe_3O_4 composite. The non-functionalized iron(II,III) oxide nanopowder (97% trace metals) with a particle diameter (50–100) nm was purchased from Millipore Sigma. All reagents and solvents were used as received.

The desired molecular structures were verified through vibrational mode identification using infrared spectroscopy (figure 1) and x-ray diffraction (supplementary figure 1). The infrared spectra were collected with a Nicolet iS50 Fourier Transform Infrared spectrometer equipped with a SmartPerformer attenuated total reflectance accessory with a diamond crystal. The data are consistent with previously reported results for $[\text{Fe}(\text{Htrz})_2(\text{trz})](\text{BF}_4)$ (figure 1(a)) [30–32]. The prominent double-peak at 1063 cm^{-1} and 1037 cm^{-1} indicates bonding between Fe(II) and the 1,2,4-triazole ring. Smaller resonances between 3000 cm^{-1} and 3300 cm^{-1} are associated with N–H stretching. The two ring torsion peaks located at 680 cm^{-1} and 633 cm^{-1} are due to the Htrz and trz ligands arranged around the Fe atom in nominally C_{2v} symmetry [30]. For reference, the existence of a single absorption peak between 600 cm^{-1} and 700 cm^{-1} would have indicated only one type of ligand, typically Htrz, bonding with Fe(II). The addition of PANI to $[\text{Fe}(\text{Htrz})_2(\text{trz})](\text{BF}_4)$ alters the vibrational modes of both components corroborating an actual chemical composite instead of a mere mixture (figure 1(b)). Both benzenoid and quinoid ring vibrations for PANI are present at 1560 cm^{-1} and 1459 cm^{-1} , respectively. The pronounced benzenoid band combined with the mode softening of both bands to lower energy indicates a stabilization of the benzenoid structures through interaction with $[\text{Fe}(\text{Htrz})_2(\text{trz})](\text{BF}_4)$. The N–H stretch associated with PANI at around 3300 cm^{-1} is suppressed in $[\text{Fe}(\text{Htrz})_2(\text{trz})](\text{BF}_4)$ plus PANI likely due to charge transfer interactions previously observed in samples of PANI and multiwalled carbon nanotubes [33]. Its intensity is proportional to the extent of H-bonding, which is expected to weaken in $[\text{Fe}(\text{Htrz})_2(\text{trz})](\text{BF}_4)$ plus PANI contrary to experiment. The interaction between $[\text{Fe}(\text{Htrz})_2(\text{trz})](\text{BF}_4)$ and PANI softens the vibrational modes of the double-peak 1063 cm^{-1} (1037 cm^{-1}) to 1060 cm^{-1} (1030 cm^{-1}). The Fe_3O_4 nanoparticles reverse, to a great extent, these

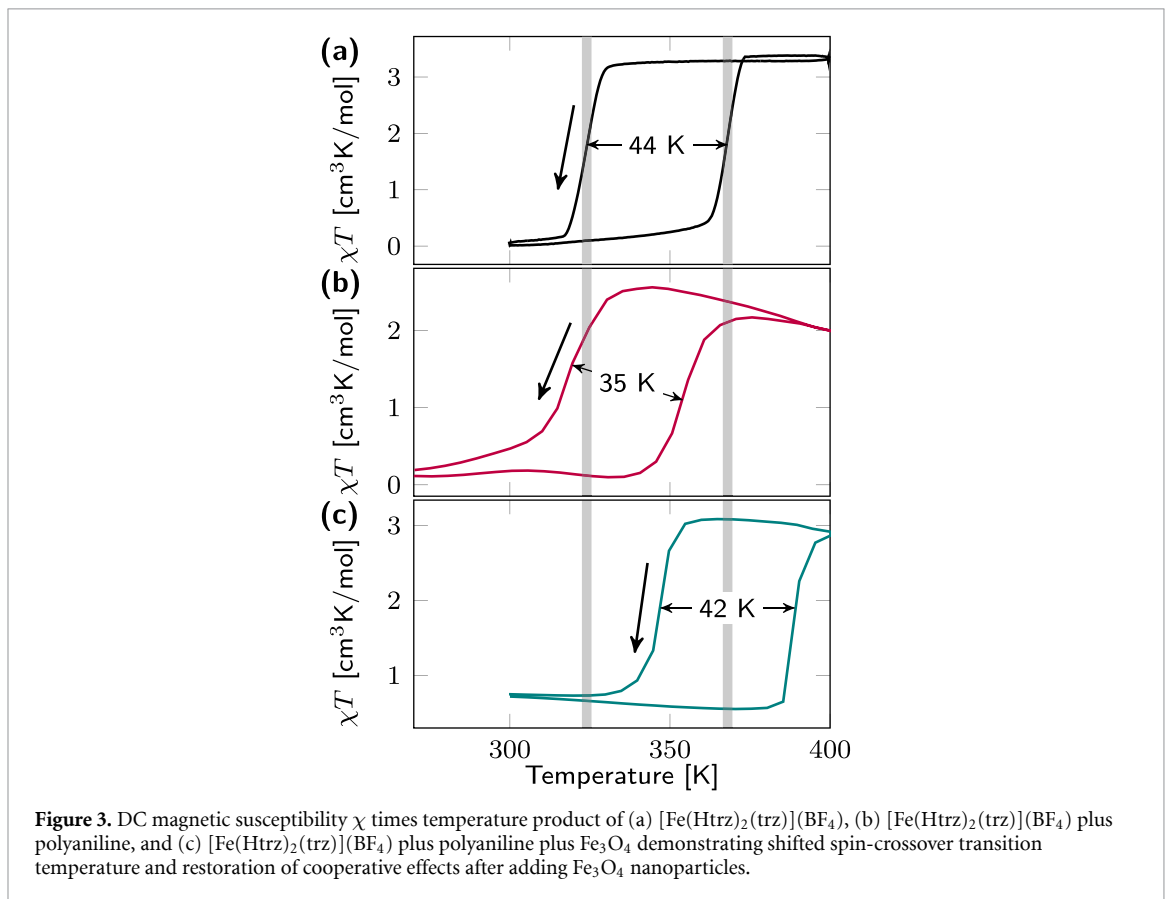
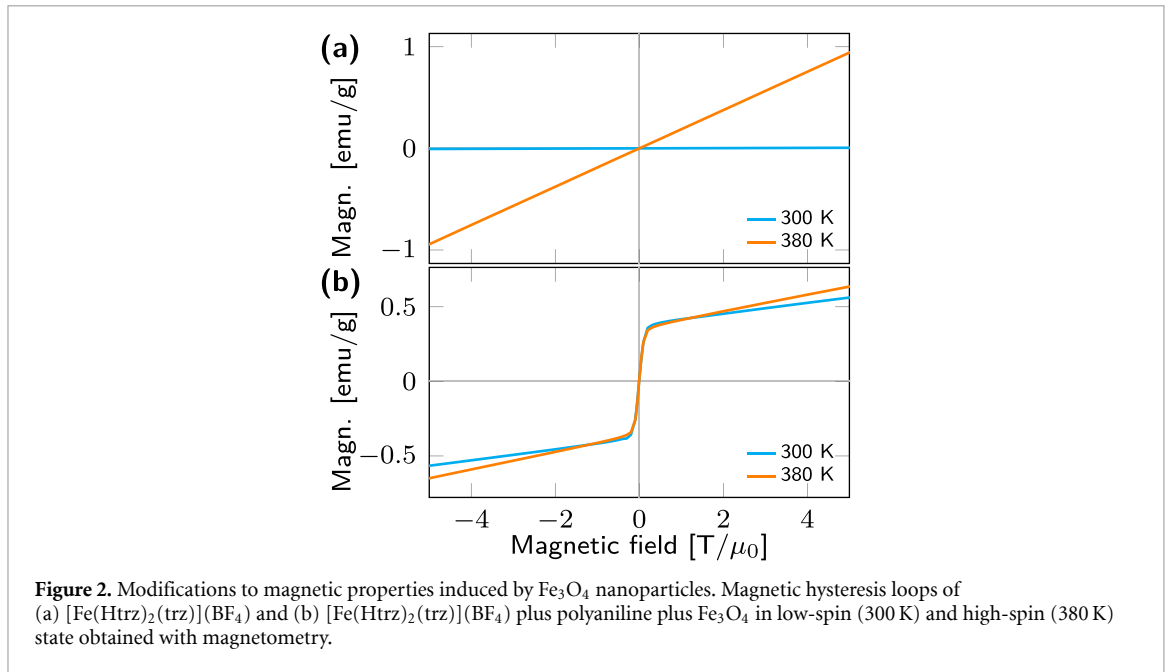


modifications by weakening the interaction between PANI and $[\text{Fe}(\text{Htrz})_2(\text{trz})](\text{BF}_4)$ (figure 1(c)). As experimentally confirmed below, this is caused by a phase separation of $[\text{Fe}(\text{Htrz})_2(\text{trz})](\text{BF}_4)$ and PANI, turning miscible into immiscible polymers. Both ring torsion peaks, which were nearly completely suppressed in $[\text{Fe}(\text{Htrz})_2(\text{trz})](\text{BF}_4)$ plus PANI, reemerge at 678 cm^{-1} and 630 cm^{-1} . The intensity of the double-peak vibrational modes increases three-fold with a slight preference for the 1030 cm^{-1} resonance, contrary to pure $[\text{Fe}(\text{Htrz})_2(\text{trz})](\text{BF}_4)$. Moreover, the benzenoid and quinoid ring vibrations are shifted to slightly higher energy, i.e. 1561 cm^{-1} and 1492 cm^{-1} , respectively, and the quinoid ring vibrational mode is as enhanced as in pure $[\text{Fe}(\text{Htrz})_2(\text{trz})](\text{BF}_4)$. The N–H stretch modes in PANI (3200 cm^{-1}) and $[\text{Fe}(\text{Htrz})_2(\text{trz})](\text{BF}_4)$ ($3000\text{--}3200\text{ cm}^{-1}$) [20] are restored.

3. Magnetization and magnetic interactions

The close proximity of ligands to the Fe metal center and corresponding crystal field effect in $[\text{Fe}(\text{Htrz})_2(\text{trz})](\text{BF}_4)$ causes orbital hybridization splitting the Fe $3d$ orbital into t_{2g} and e_g states [34]. In the low-spin state, the six electrons pair up in the t_{2g} orbital ($S = 0$) leading to diamagnetic behavior [35] at around 300 K [8–12, 15–20]. At 380 K , a spin-crossover transition occurs from the t_{2g} to the e_g orbital ($S = 2$) that is responsible for paramagnetic properties observed in the magnetic hysteresis curves (figure 2(a)). The latter were obtained for powder samples using superconducting quantum interference device magnetometry with a Quantum Design Magnetic Properties Measurement System. Adding Fe_3O_4 nanoparticles to $[\text{Fe}(\text{Htrz})_2(\text{trz})](\text{BF}_4)$ plus PANI yields unsurprisingly a magnetization even in the low-spin state (figure 2(b)), which is characteristic of superparamagnetism [1]. Both low-spin and high-spin state reveal a non-vanishing high-field magnetic susceptibility (paramagnetism). The low-spin state paramagnetism suggests an exchange coupling between $[\text{Fe}(\text{Htrz})_2(\text{trz})](\text{BF}_4)$ and Fe_3O_4 . The large local moment of Fe in the high-spin state results in a stronger paramagnetic contribution of disordered spin-crossover molecules. Given the weight ratio of $25 : 25 : 0.5$ for $[\text{Fe}(\text{Htrz})_2(\text{trz})](\text{BF}_4)$ plus PANI plus Fe_3O_4 , we estimate a magnetic susceptibility for the spin-crossover molecules that is 15% of that of pure $[\text{Fe}(\text{Htrz})_2(\text{trz})](\text{BF}_4)$. The lack of a magnetic hysteresis, i.e. sizable coercive field, suggests a weak, if not absent, magnetostatic interaction between sparsely dense Fe_3O_4 nanoparticles. In contrast, assemblies of closely packed carboxylated Fe_3O_4 nanoparticles with separations $\lesssim 5\text{ nm}$ become ferromagnetic [1].

The role of magnetic intermolecular interactions and cooperative effects is examined in terms of the thermal hysteresis of χT (the product of magnetic susceptibility and temperature) between low-spin and high-spin state. $[\text{Fe}(\text{Htrz})_2(\text{trz})](\text{BF}_4)$ possesses a thermal hysteresis with a width of 44 K (figure 3(a)) corroborating cooperative effects due to significant intermolecular interaction. The addition of PANI lowers, in particular, the warming transition temperature (resulting in a smaller hysteresis) and causes an overall less steep transition (figure 3(b)). The corresponding weakening of cooperative effects can be explained by the



increased separation of individual $[\text{Fe}(\text{Htrz})_2(\text{trz})](\text{BF}_4)$ molecules due to intermixing with PANI. Markedly, the intermolecular coupling is restored through the presence of Fe_3O_4 nanoparticles resulting in an as wide thermal hysteresis as for pure $[\text{Fe}(\text{Htrz})_2(\text{trz})](\text{BF}_4)$ that is shifted by 20 K to higher temperatures (figure 3(c)). This modification infers some kind of coupling between Fe_3O_4 nanoparticles and $[\text{Fe}(\text{Htrz})_2(\text{trz})](\text{BF}_4)$ mediated by an inherent nanoparticle functionalization and orbital bonding to the spin-crossover molecule and phase separation between the $[\text{Fe}(\text{Htrz})_2(\text{trz})](\text{BF}_4)$ and PANI, as discussed below.

Even aging, i.e. exposing the samples to ambient conditions for weeks, preserves the thermal hysteresis. For $[\text{Fe}(\text{Htrz})_2(\text{trz})](\text{BF}_4)$ films, this pertains to a width of 40 K and rectangular shape that coincide with

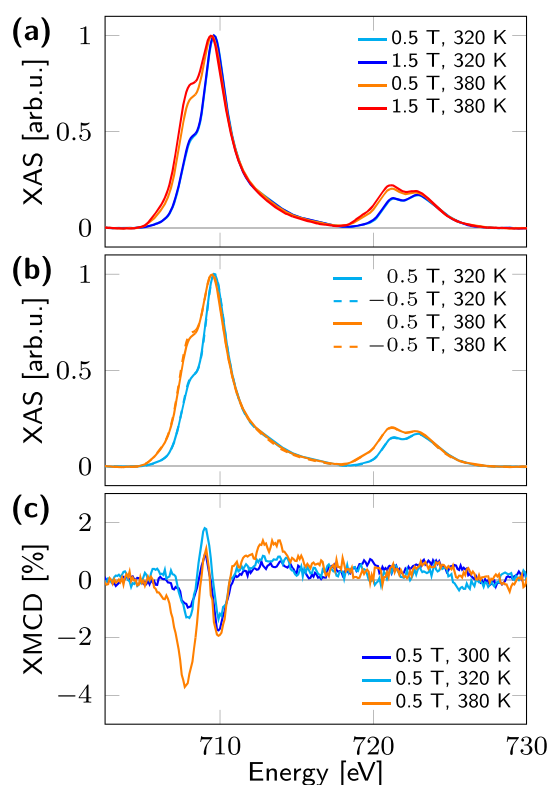


Figure 4. X-ray absorption (XAS) and x-ray magnetic circular dichroism (XMCD) spectroscopy of $[\text{Fe}(\text{Htrz})_2(\text{trz})](\text{BF}_4)$ plus polyaniline plus Fe_3O_4 films. (a) Absorption spectra in the low-spin (320 K) and high-spin (380 K) state at different normal magnetic bias fields revealing field dependence of high-spin state due to its incomplete population. (b) Absorption spectra taken with circularly polarized light at positive and negative magnetic bias unveiling marginal difference. (c) Corresponding XMCD spectra characteristic of trivalent Fe in Fe_3O_4 with sizable contribution of high-spin state corroborating ferromagnetic coupling between the two components.

freshly made films (supplementary figure 2). $[\text{Fe}(\text{Htrz})_2(\text{trz})](\text{BF}_4)$ plus PANI and $[\text{Fe}(\text{Htrz})_2(\text{trz})](\text{BF}_4)$ plus PANI plus Fe_3O_4 exhibit somewhat deformed thermal hysteresis loops. The latter composite retains its large width indicating that the morphological change driven by the addition of Fe_3O_4 nanoparticles causes an equilibrium phase separation (discussed below) and interactions between $[\text{Fe}(\text{Htrz})_2(\text{trz})](\text{BF}_4)$ and the Fe_3O_4 nanoparticles.

The coupling between $[\text{Fe}(\text{Htrz})_2(\text{trz})](\text{BF}_4)$ and Fe_3O_4 was further examined with x-ray absorption and XMCD spectroscopies at beamline 6.3.1 (Advanced Light Source, Berkeley, CA). Using total electron yield and circularly polarized x-rays with an estimated degree of polarization of 0.66, the x-ray absorption spectra of films, obtained by drop-casting a solution of $[\text{Fe}(\text{Htrz})_2(\text{trz})](\text{BF}_4)$ plus PANI plus Fe_3O_4 on a highly oriented pyrolytic graphite (HOPG) substrate, were recorded around the Fe $L_{3,2}$ edges. The absorption spectra of composites in the low-spin state are unaffected by the presence of a magnetic field and look similar to prior reports on Fe_3O_4 [36, 37] where the 708.1 eV peak is roughly 55% in height of the 709.5 eV peak, indicating primarily trivalent Fe (figures 4(a) and (b)). The pre-edge shoulders unique to Fe_3O_4 and FeO are also observed. The enhanced x-ray absorption at 708.1 eV is due to an increased high-spin state population near the spin-crossover transition temperature and not unexpected as the applied magnetic field can lower the activation barriers to the high-spin state [38–41]. As evident from the thermal hysteresis (figure 3(c)), a temperature of 380 K is insufficient to completely populate the high-spin state at remanence. This conclusion is supported by a marginal change of the XMCD signal with magnetic field in the high-spin state. The absorption spectra in the low-spin state are identical for magnetic fields in the range of $(-1.5 \sim 1.5) \text{ T}/\mu_0$. Comparison with literature [42–44] reveals a mixture of divalent and trivalent Fe in Fe_3O_4 since neither the first (707.8 eV) nor the second (710.0 eV) dip in the XMCD signal dominates (figure 4(c)). The increase in magnitude at 707.8 eV at elevated temperature originates from the local Fe moment of $[\text{Fe}(\text{Htrz})_2(\text{trz})](\text{BF}_4)$ and corroborates ferromagnetic coupling between $[\text{Fe}(\text{Htrz})_2(\text{trz})](\text{BF}_4)$ and Fe_3O_4 . A similar ferromagnetic coupling was reported for spin-crossover Fe octaethylporphyrin complexes on oxidized nickel and cobalt surfaces [45].

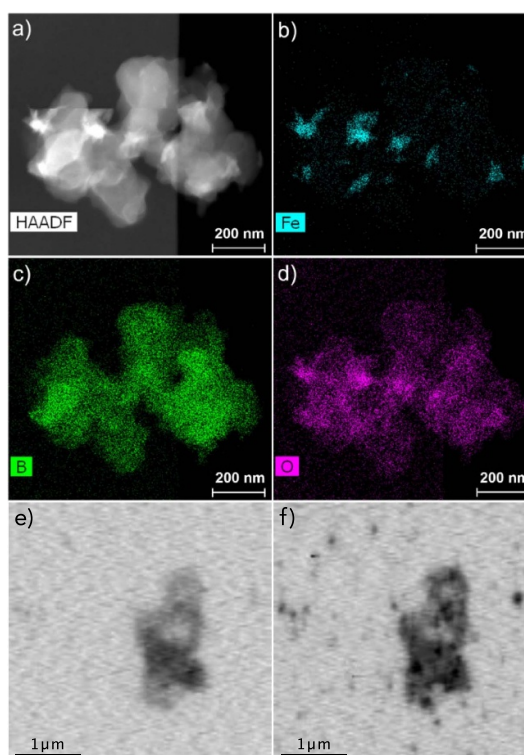


Figure 5. Elemental mapping of $[\text{Fe}(\text{Htrz})_2(\text{trz})](\text{BF}_4)$ plus polyaniline plus Fe_3O_4 with scanning transmission electron and x-ray microscopies. (a) Agglomerate visualized with scanning transmission electron microscopy operated in high-angle annular dark-field imaging mode and corresponding elemental maps for (b) iron, (c) boron, and (d) oxygen. (e) Spatially resolved x-ray transmission of (e) unoccupied $\text{Fe } t_{2g}$ orbitals in $[\text{Fe}(\text{Htrz})_2(\text{trz})](\text{BF}_4)$ (706 eV) and (f) Fe_3O_4 (709 eV). Dark regions highlight location of high concentration.

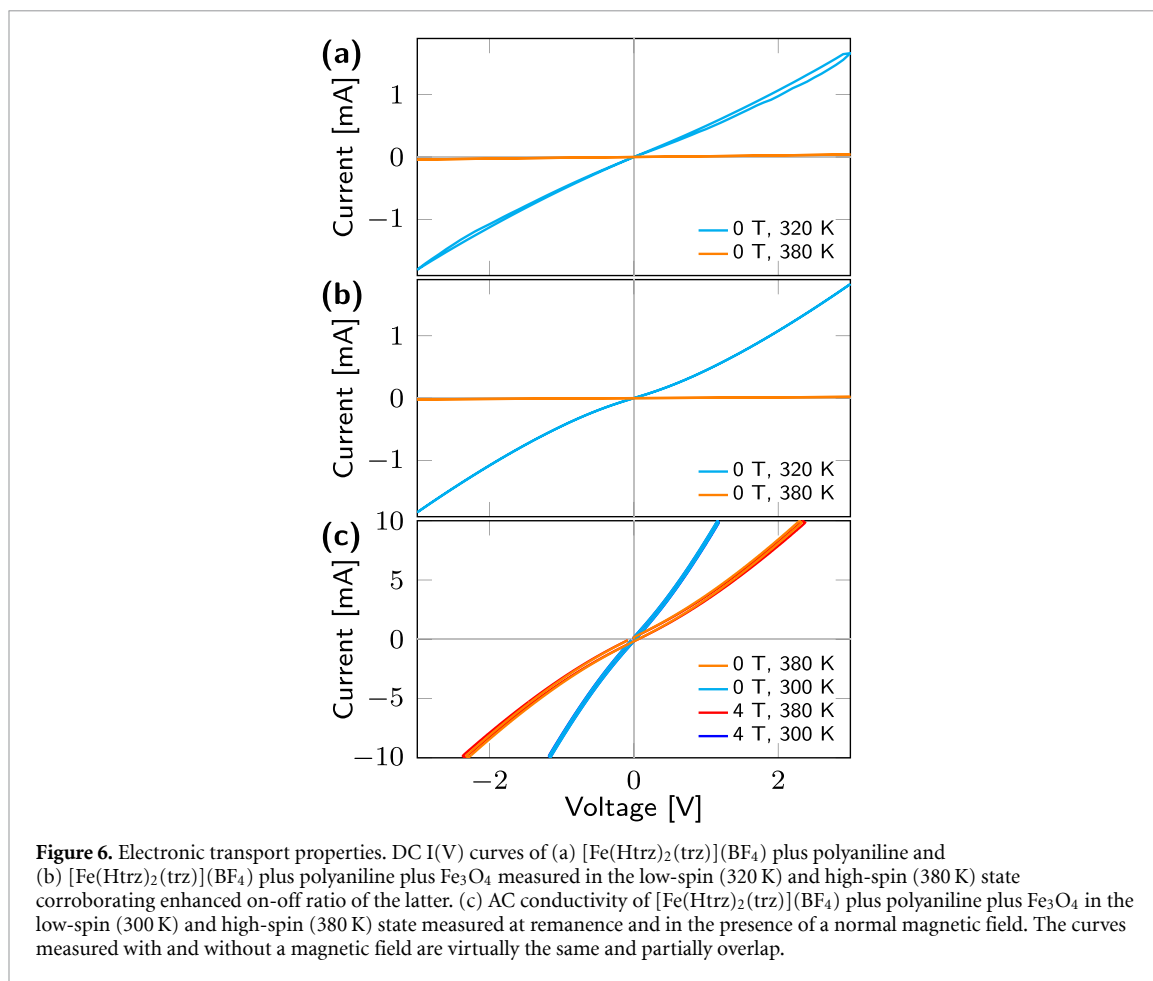
4. Phase separation

The phase separation of $[\text{Fe}(\text{Htrz})_2(\text{trz})](\text{BF}_4)$, PANI, and Fe_3O_4 nanoparticles was investigated at room temperature by means of high-angle annular dark field-scanning transmission electron microscopy with energy-dispersive x-ray spectroscopy using an FEI Tecnai Osiris (S)TEM (figures 5(a)–(d)). Elemental mapping of iron, boron, and oxygen unveils a phase separation of $[\text{Fe}(\text{Htrz})_2(\text{trz})](\text{BF}_4)$ and PANI, which is consistent with the aforementioned thermal hysteresis measurements and infrared absorption spectra. Scanning transmission x-ray microscopy with a photon energy tuned to the $\text{Fe } L_3$ edge probing $[\text{Fe}(\text{Htrz})_2(\text{trz})](\text{BF}_4)$ Fe-weighted t_{2g} molecular orbitals (≈ 706 eV) and Fe–O (≈ 709 eV) enabled the differentiation between Fe_3O_4 and $[\text{Fe}(\text{Htrz})_2(\text{trz})](\text{BF}_4)$. The majority of Fe_3O_4 nanoparticles is confined to $[\text{Fe}(\text{Htrz})_2(\text{trz})](\text{BF}_4)$, though smaller agglomerates exist in PANI (figures 5(e) and (f)). These measurements were conducted at the COSMIC beamline 7.0.1.2 (Advanced Light Source, Berkeley, CA) using linearly polarized photons. For both samples, solutions of $[\text{Fe}(\text{Htrz})_2(\text{trz})](\text{BF}_4)$ plus PANI plus Fe_3O_4 were drop-casted on standard silicon nitride transmission electron microscopy membranes (Norcada) with a $(0.5 \times 0.5) \text{ mm}^2$ window.

The phase separation directly affects the morphology and homogeneity of the drop-casted films. Scanning electron microscopy with an in-lens detector on $[\text{Fe}(\text{Htrz})_2(\text{trz})](\text{BF}_4)$ plus PANI plus Fe_3O_4 (1 weight-%) revealed a continuous inhomogeneous film with significant clustering and percolation (supplementary figure 3). These imperfections become more prominent with increasing nanoparticle concentration and enhance contributions from extrinsic properties that are undesirable for our study.

5. Electronic transport properties

The DC current–voltage $I(V)$ characteristics of $[\text{Fe}(\text{Htrz})_2(\text{trz})](\text{BF}_4)$ plus PANI are compared with the $[\text{Fe}(\text{Htrz})_2(\text{trz})](\text{BF}_4)$ plus PANI plus Fe_3O_4 nanoparticles in figures 6(a) and (b). The temperature-dependent DC $I(V)$ measurements were performed on dried solutions of $[\text{Fe}(\text{Htrz})_2(\text{trz})](\text{BF}_4)$ plus PANI plus Fe_3O_4 drop-casted on an organic field-effect transistor template manufactured by the Fraunhofer-Institut für Photonische Mikrosysteme (IPMS). The $I(V)$ curves were recorded with a 4200 A SCS parameter analyzer connected to a Lakeshore cryogenic probe station. Both films possess a higher



conductivity than pure $[\text{Fe}(\text{Htrz})_2(\text{trz})](\text{BF}_4)$ [19, 21], and the lower conductivity in the high-spin state is consistent with prior reports [9, 16, 18, 19]. The nonlinearity of the conductivity in the low-spin state indicates additional free charge carriers that are added by the Fe_3O_4 nanoparticles to the conduction channel at high bias voltages. In addition, the resistivity of the high-spin state is markedly enhanced (factor of 2). The combination of all these characteristics indicates a conduction through both PANI and $[\text{Fe}(\text{Htrz})_2(\text{trz})](\text{BF}_4)$ molecules with magnetite nanoparticles despite the phase separation and inhomogeneity of the films.

This conclusion is corroborated by the AC electronic transport properties. Samples for AC measurements were fabricated by drop-casting a solution of $[\text{Fe}(\text{Htrz})_2(\text{trz})](\text{BF}_4)$ plus PANI plus Fe_3O_4 in an interdigitated electrode (Metrohm Dropsens) and stored for more than four weeks in an ultra-high vacuum chamber to degas. The AC I(V) curves were obtained in 2-point in-plane geometry using a Quantum Design DynaCool Physical Properties Measurement System at an excitation frequency of 97.6 Hz. The AC conductivity of $[\text{Fe}(\text{Htrz})_2(\text{trz})](\text{BF}_4)$ plus PANI plus Fe_3O_4 exceeds that of pure $[\text{Fe}(\text{Htrz})_2(\text{trz})](\text{BF}_4)$ [18] by several orders of magnitude (figure 6(c)). In addition, the conductivity in the low-spin state is higher than in the high-spin state without a noticeable dependence on the magnetic bias field (up to $4 \text{ T}/\mu_0$) and Fe_3O_4 nanoparticles. A conduction through PANI alone would yield larger, virtually temperature-independent conductivity values. Compared with DC measurements, the AC conductivity in the low-spin state is 20 times larger at the expense of a reduced on-off ratio. This illustrates that the short-range conductivity is larger than the long-range conductivity.

6. Conclusion

We synthesized composite films of $[\text{Fe}(\text{Htrz})_2(\text{trz})](\text{BF}_4)$ plus PANI plus Fe_3O_4 nanoparticles and compared molecular structure, morphology, magnetic properties, and electronic transport to $[\text{Fe}(\text{Htrz})_2(\text{trz})](\text{BF}_4)$ films with and without PANI. The addition of Fe_3O_4 nanoparticles causes a phase separation of $[\text{Fe}(\text{Htrz})_2(\text{trz})](\text{BF}_4)$ and PANI that restores cooperative effects between the spin-crossover molecules. The observation of ferromagnetic exchange coupling between $[\text{Fe}(\text{Htrz})_2(\text{trz})](\text{BF}_4)$ and Fe_3O_4 nanoparticles by means of XMCD spectroscopy infers an inherent functionalization of the originally non-functionalized nanoparticles and chemical bonding to the molecules. The use of low-concentration nanoparticles (1

weight-%) increases the on-off ratio of DC conductivity by enlarging the resistivity of the high-spin state (off state) and leads to an AC conductivity of the on state that is 20 times larger than the DC on state. Given the stark morphological differences between $[\text{Fe}(\text{Htrz})_2(\text{trz})](\text{BF}_4)$ plus PANI with and without Fe_3O_4 nanoparticles, the preservation of high AC and DC conductivity of the low-spin state is striking. Manipulating cooperative effects through the presence of superparamagnetic nanoparticles may open a new avenue for tailoring electronic transport properties of spin-crossover systems and prospective applications of composite materials in microelectronics, particularly where high resistivity has been a major concern.



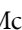
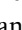


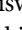

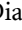
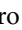


Data availability statement

All data that support the findings of this study are included within the article (and any supplementary files).

Acknowledgments

This research was supported by the National Science Foundation through NSF-DMR Grant No. 2003057 [T K Ekanayaka, WaiKiat Chin, M Zaid Zaz, Gauthami Viswan, P A Dowben], NSF-DMR Grant No. 2203933 [R Zielinski, R Streubel], NSF-DMR Grant No. 1827690 [R Y Lai, K A McElveen, E Mishra], and EPSCoR RII Track-1: Emergent Quantum Materials and Technologies (EQUATE), Award OIA-2044049 [R Y Lai, K M McElveen]. The research was performed in part at the Nebraska Nanoscale Facility: National Nanotechnology Coordinated Infrastructure which supported by the National Science Foundation under Award No. ECCS: 1542182. This research used resources of the Advanced Light Source, which is a DOE Office of Science User Facility under Contract No. DE-AC02-05-CH11231. The authors thank Bing Qiang Wei from Mechanical and Material Engineering at the University of Nebraska-Lincoln for the technical support with HAADF-STEM.

ORCID iDs

Esha Mishra  <https://orcid.org/0000-0002-8317-9370>
WaiKiat Chin  <https://orcid.org/0000-0002-1840-0825>
Kayleigh A McElveen  <https://orcid.org/0000-0002-1030-2913>
Thilini K Ekanayaka  <https://orcid.org/0000-0003-3650-0210>
M Zaid Zaz  <https://orcid.org/0000-0001-7849-4715>
Gauthami Viswan  <https://orcid.org/0000-0002-6241-5426>
Ruthi Zielinski  <https://orcid.org/0000-0003-3719-0699>
Alpha T N'Diaye  <https://orcid.org/0000-0001-9429-9776>
David Shapiro  <https://orcid.org/0000-0002-4186-6017>
Rebecca Y Lai  <https://orcid.org/0000-0002-1732-9481>
Robert Streubel  <https://orcid.org/0000-0003-4783-892X>
Peter A Dowben  <https://orcid.org/0000-0002-2198-4710>

References

- [1] Liu X et al 2019 *Science* **365** 264
- [2] Prabhakaran T and Hemalatha J 2016 *RSC Adv.* **6** 86880
- [3] Behera C, Choudhary R N P and Das P R 2017 *J. Polym. Res.* **24** 56
- [4] Rana D K, Singh S K, Kundu S K, Roy S, Angappane S and Basu S 2019 *New J. Chem.* **43** 3128–38
- [5] Senthil Kumar K and Ruben M 2017 *Coord. Chem. Rev.* **346** 176–205
- [6] Molnár G, Rat S, Salmon L, Nicolazzi W and Bousseksou A 2018 *Adv. Mater.* **30** 1703862
- [7] Enriquez-Cabrera A, Rapakousiou A, Piedrahita Bello M, Molnár G, Salmon L and Bousseksou A 2020 *Coord. Chem. Rev.* **419** 213396
- [8] Faulmann C, Chahine J, Malfant I, de Caro D, Cormary B and Valade L 2011 *Dalton Trans.* **40** 2480
- [9] Rotaru A, Gural'skiy I A, Molnar G, Salmon L, Demont P and Bousseksou A 2012 *Chem. Commun.* **48** 4163
- [10] Lefter C, Tan R, Dugay J, Tricard S, Molnar G, Salmon L, Carrey J, Nicolazzi W, Rotaru A and Bousseksou A 2016 *Chem. Phys. Lett.* **644** 138
- [11] Grosjean A, Daro N, Pechev S, Etrillard C, Chastanet G and Guionneau P 2018 *Eur. J. Inorg. Chem.* **2018** 429
- [12] Siddiqui S A, Domanov O, Schaffer E, Vejpravova J and Shiozawa H 2021 *J. Mater. Chem. C* **9** 1077
- [13] Voisin H, Aimé C, Vallée A, Bleuzen A, Schmutz M, Mosser G, Coradin T and Roux C 2017 *J. Mater. Chem. C* **5** 11542
- [14] Voisin H, Aimé C, Vallée A, Coradin T and Roux C 2018 *Inorg. Chem. Front.* **5** 2140
- [15] Rotaru A, Dugay J, Tan R P, Gural'skiy I A, Salmon L, Demont P, Carrey J, Molnár G, Respaud M and Bousseksou A 2013 *Adv. Mater.* **25** 1745
- [16] Lefter C, Gural'skiy I A, Peng H, Molnár G, Salmon L, Rotaru A, Bousseksou A and Demont P 2014 *Phys. Status Solidi* **8** 191–3
- [17] Dugay J, Giménez-Marqués M, Kozlova T, Zandbergen H W, Coronado E and van der Zant H S J 2015 *Adv. Mater.* **27** 1288
- [18] Lefter C, Tricard S, Peng H, Molnár G, Salmon L, Demont P, Rotaru A and Bousseksou A 2015 *J. Phys. Chem. C* **119** 8522
- [19] Mishra E, Ekanayaka T K, McElveen K A, Lai R Y and Dowben P A 2022 *Org. Electron.* **105** 106516

- [20] Kroeber J, Audiere J P, Claude R, Codjovi E, Kahn O, Haasnoot J G, Groliere F, Jay C and Bousseksou A 1994 *Chem. Mater.* **6** 1404
- [21] Nieto-Castro D, Garcés-Pineda F A, Moneo-Corcuera A, Sánchez-Molina I and Galán-Mascarós J R 2021 *Adv. Funct. Mater.* **31** 2102469
- [22] Koo Y S and Galán-Mascarós J R 2014 *Adv. Mater.* **26** 6785
- [23] Ekanayaka T K et al 2021 *Magnetochemistry* **7** 37
- [24] Kipgen L et al 2018 *Nat. Commun.* **9** 2984
- [25] Félix G, Nicolazzi W, Salmon L, Molnár G, Perrier M, Maurin G, Larionova J, Long J, Guari Y and Bousseksou A 2013 *Phys. Rev. Lett.* **110** 235701
- [26] Bauer W, Lochenie C and Weber B 2014 *Dalton Trans.* **43** 1990
- [27] Jiang X et al 2019 *J. Phys.: Condens. Matter* **31** 315401
- [28] Tang S J, Wang A T, Lin S Y, Huang K Y, Yang C C, Yeh J M and Chiu K C 2011 *Polym. J.* **43** 667
- [29] Adams D M and Hendrickson D N 1996 *J. Am. Chem. Soc.* **118** 11515–28
- [30] Haasnoot J G, Vos G and Groeneveld W L 1977 *Z. Naturforsch. B* **32** 1421
- [31] Diaconu A, Lupu S L, Rusu I, Risca I M, Salmon L, Molnár G, Bousseksou A, Demont P and Rotaru A 2017 *J. Phys. Chem. Lett.* **8** 3147
- [32] Nguyen T A D, Veauthier J M, Angles-Tamayo G F, Chavez D E, Lapsheva E, Myers T W, Nelson T R and Schelter E J 2020 *J. Am. Chem. Soc.* **142** 4842–51
- [33] Cochet M, Maser W K, Benito A M, Callejas M A, Martínez M T, Benoit J M, Schreiber J and Chauvet O 2001 *Chem. Commun.* **16** 1450–1
- [34] Weber B 2014 *Koordinationschemie: Grundlagen und Aktuelle Trends* (Springer)
- [35] Zhang X, Palamarciuc T, Létard J F, Rosa P, Lozada E V, Torres F, Rosa L G, Doudin B and Dowben P A 2014 *Chem. Commun.* **50** 2255
- [36] Regan T J, Ohldag H, Stamm C, Nolting F, Lüning J, Stöhr J and White R L 2001 *Phys. Rev. B* **64** 214422
- [37] Kuepper K, Balasz I, Hesse H, Winiarski A, Prince K C, Matteucci M, Wett D, Szargan R, Burzo E and Neumann M 2004 *Phys. Status Solidi a* **201** 3252–6
- [38] Bousseksou A, Negre N, Goiran M, Salmon L, Tuchagues J P, Boillot M L, Boukheddaden K and Varret F 2000 *Eur. Phys. J. B* **13** 451–6
- [39] Jakobsen V B et al 2021 *Inorg. Chem.* **60** 6167–75 PMID: 33331784
- [40] Zhang X et al 2017 *Adv. Mater.* **29** 1702257
- [41] Hao G et al 2021 *Magnetochemistry* **7** 135
- [42] Huang D J, Chang C F, Jeng H T, Guo G Y, Lin H J, Wu W B, Ku H C, Fujimori A, Takahashi Y and Chen C T 2004 *Phys. Rev. Lett.* **93** 077204
- [43] Pilard M, Ersen O, Cherifi S, Carvello B, Roiban L, Muller B, Scheurer F, Ranno L and Boeglin C 2007 *Phys. Rev. B* **76** 214436
- [44] Lee E et al 2013 *Appl. Phys. Lett.* **102** 133703
- [45] Bernien M et al 2009 *Phys. Rev. Lett.* **102** 047202